Climatology of Tropical Intraseasonal Convective Anomalies: 1979–2002

CHARLES JONES

Institute for Computational Earth System Science, University of California, Santa Barbara, Santa Barbara, California

LEILA M. V. CARVALHO

Department of Atmospheric Sciences, Institute of Astronomy, Geophysics and Atmospheric Sciences, University of São Paulo, São Paulo, Brazil

R. WAYNE HIGGINS

NOAA/NWS/NCEP/Climate Prediction Center, Washington, D.C.

DUANE E. WALISER

Institute for Terrestrial and Planetary Atmospheres, State University of New York at Stony Brook, Stony Brook, New York

J.-K. E. SCHEMM

NOAA/NWS/NCEP/Climate Prediction Center, Washington, D.C.

(Manuscript received 6 August 2002, in final form 9 July 2003)

ABSTRACT

Tropical intraseasonal convective anomalies (TICA) have a central role in subseasonal changes in the coupled ocean–atmosphere system, but the climatology of TICA events has not been properly documented. This study exploits 24 years of outgoing longwave radiation (OLR) data and a tracking algorithm to develop a climatology of eastward propagating TICA events. Three distinct types of TICA occurrences are documented according to their propagation characteristics. The first type (IND) is characterized by events that propagate in the Indian Ocean without significant influence in the western Pacific Ocean. The second and third types are associated with occurrences of the Madden–Julian oscillation during boreal winters (MJO) and summers (ISO). The frequency of occurrence of TICA events is highest in April–June and October–December and lowest in July–September. An analysis of the spatial and temporal characteristics reveals that MJO events tend to have the longest life cycle, greatest intensity, and largest variability inside the contiguous region of OLR anomaly. Given the data record of 24 years, the analysis of interannual occurrences of TICA events does not show statistically significant differences among events that occur in different phases of the El Niño–Southern Oscillation (ENSO). A procedure is developed to identify major MJO events and estimate their frequency of occurrence in the data record.

1. Introduction

It is widely recognized that tropical intraseasonal oscillations have a significant role in global-scale precipitation changes and involve important mechanisms of low-frequency variability in the climate system (Rasmusson and Arkin 1993). On this time scale (roughly 10 to 90 days), the Madden–Julian oscillation (MJO) stands out as the dominant mode of tropical intraseasonal variability and is most active in the boreal winter (Madden and Julian 1994). We refer to boreal winter occurrences as MJO and boreal summer events as ''intraseasonal oscillation'' (ISO) simply to differentiate the seasonality of the MJO. The influences of the MJO (ISO) on the patterns of precipitation in the global Tropics and in portions of the extratropics have been well documented. For example, the MJO (ISO) strongly influences the precipitation patterns associated with the monsoons in Asia–Australia, and moderately in North America and South America (Yasunari 1979; Lau and Chan 1986; Mo 2000; Nogués-Paegle et al. 2000; Higgins and Shi 2001; Jones and Carvalho 2002). This influence has been shown to modulate rainfall variability and extreme events in the Americas as well (Higgins et al. 2000; Jones 2000; Carvalho et al. 2004). From a practical point of view, some studies have also indicated that the interaction of the MJO with the extratropical

Corresponding author address: Dr. Charles Jones, Institute for Computational Earth System Science, University of California, Santa Barbara, Santa Barbara, CA 93106.
E-mail: cjones@icess.ucsb.edu

regions can influence weather forecasts on medium and extended ranges (Ferranti et al. 1990; Lau and Chang 1992).

An important characteristic of the MJO is its high degree of case-to-case variability as well as its seasonal to interannual variations (Weickmann 1991; Madden and Julian 1994; Slingo et al. 1999). The MJO (ISO) is usually identified with satellite data, given the significant variations that occur in tropical convection during its life cycle. The purpose of this paper is to obtain an updated climatology of tropical intraseasonal convective anomalies (TICA) using 24 years of outgoing longwave radiation data. By using a tracking algorithm of tropical convective regions, we characterize the occurrences of TICA events and their properties. The specific questions addressed are: what is the *seasonal frequency* of MJO (ISO) *occurrences?* How does the *frequency* of MJO (ISO) *occurrences* depend on the *phase of* El Niño–Southern Oscillation (ENSO)? Is the *evolution* of MJO and ISO events *significantly different* in terms of *intensity* and *propagation speeds?* Furthermore, an important issue examined in this study is the frequency of major MJO events and identification of major MJO occurrences with significant low-level wind anomalies in the western Pacific region.

In the context above, it is useful to review the results of Wang and Rui (1990) since they are pertinent to this study. Wang and Rui (1990, hereafter WR) developed a limited climatology of TICA occurrences using nine years of outgoing longwave radiation (OLR). In their approach, the annual and interannual components of pentad-mean OLR were removed, and TICA events were identified by tracking the temporal evolution of negative OLR anomalies. OLR features were required to have a life span of at least four pentads. During the life span, the zonal dimension of the OLR features was required to exceed 30° in longitude and the central OLR anomaly needed to be less than -15 W m^{-2}. Furthermore, at the strongest stage during the evolution, the zonal dimension was required to exceed 50° in longitude and the minimum OLR to be less than -25 W m^{-2}. TICA geographical locations and their propagation characteristics were obtained by tracking the grid point with the lowest OLR anomaly. The examination of the propagation characteristics revealed a multitude of behaviors such as eastward, westward, and northward movement. This led WR to propose three types of propagation characteristics: equatorial eastward (EE), eastward propagation with north and/or south movement (N/S–E) and eastward propagation with northward movement (EN) (see their Fig. 5 for details). TICA seasonality, as well as some of their characteristics (intensity, duration, and speed), was discussed. However, the limited number of years used in the analysis precluded the authors from examining interannual variations. Furthermore, a statistical analysis in terms of frequency of major MJO occurrences was not investigated.

In this paper we limit the analysis to *eastward* propagating events (hereafter called TICA) since they are closely related to the MJO (ISO). Second, we investigate differences in the spatial and temporal characteristics of different types of TICA events. Given the influential nature of the MJO in the coupled ocean–atmosphere system, we examine the frequency of TICA occurrences and their dependence on the seasonal cycle and phase of ENSO. The organization of this paper is as follows. Section 2 summarizes the datasets used. The methodology to identify and categorize TICA events is discussed in section 3. Seasonal variations of TICA events are discussed in section 4. Differences in TICA characteristics are presented in section 5. Interannual variations and the occurrence of major MJO events are discussed in section 6 and section 7 summarizes the results.

2. Data

The identification of TICA was performed by tracking OLR features, which are often used as a proxy for large-scale tropical convective activity (e.g., Lau and Chan 1986; Waliser et al. 1993; Jones et al. 1998). Pentads of OLR (5-day nonoverlapping means with 73 pentads per year) were used from 1–5 January 1979 through 27–31 December 2002 (1752 pentads). Additional information on changes in instrumentation, equator-crossing times, and inherent biases in the OLR data are described in Chelliah and Arkin (1992) and Lucas et al. (2001).

The spatial resolution of the OLR field was decreased to 5° × 5° to focus on the large-scale features of TICA characteristics. In order to retain intraseasonal variations, a simple filtering procedure was applied to each pentad OLR time series. First, periods longer than 100 days were filtered in frequency domain by applying fast Fourier transforms (FFT). The resulting time series was additionally smoothed with one pass of a 1–2–1 running average to decrease high-frequency oscillations. The primary reason for using this simple temporal filter procedure and not a bandpass filter is that it can be applied in real-time applications. For instance, the statistical forecast skill of TICA occurrences is further discussed in Jones et al. (2002, manuscript submitted to *J. Climate*). A comparison of this filtering procedure with OLR anomalies computed with a Lanczos bandpass filter (20–90 days) indicated correlations on the order of 0.8–0.9 over most of the Tropics. Finally, the OLR anomalies were filtered in space with a weighted-average spatial filter such that each filtered value is given by

$$\mathrm{OLR}'_j = \frac{1}{2}\mathrm{OLR}_j + \sum_{k=1}^{8} \frac{1}{8}\mathrm{OLR}_k,$$

where the summation is for the eight neighbor points of OLR_j.

3. Methodology to identify and characterize TICA occurrences

The identification and characterization of TICA occurrences involved a number of steps. First, a threshold mask of -10 W m^{-2} was applied to each pentad map of OLR anomalies, and grid points not satisfying this criterion were set to an arbitrary value (equal to zero). Next, contiguous regions with OLR anomalies less than -10 W m^{-2} were tagged in each pentad map. Only contiguous regions with sizes greater than 10 grid points ($5° \times 5°$ latitude–longitude resolution) and minimum OLR anomaly less than -15 W m^{-2} were kept for subsequent analysis. The contiguous OLR anomalies passing this initial screening process were the ones tracked in time. The tracking algorithm is insensitive to a reasonable range of minimum size of contiguous regions. Increasing the minimum size (e.g., 15 contiguous grid points) implies that potentially weak and small TICA cases can be missed from the analysis.

The tracking of the contiguous OLR anomalies was accomplished by applying a modified version of the maximum spatial correlation tracking technique (MASCOTTE) described in Carvalho and Jones (2001). That algorithm was originally developed to track the evolution of mesoscale convective systems using satellite images with high temporal and spatial resolution. The modifications introduced were minimal and only necessary to account for the different temporal and spatial resolution of the OLR anomaly data. The MASCOTTE basic hypothesis is that the spatial correlation between contiguous regions in successive images is a simple and powerful method to identify the evolution of spatial patterns.

To briefly summarize the procedure, we consider $N = 1752$ (24 yr) maps of OLR anomalies. At time t_i, there are m contiguous OLR regions. The kth contiguous region ($1 \leq k \leq m$) is first isolated (i.e., the remainder of the map is set to the background mask value). We then consider the next pentad map at time t_{i+1} and identify all the contiguous regions. The contiguous region at t_{i+1} that has maximum spatial correlation ($r_s > 0.20$) with the kth region at t_i is considered the new spatial position of the OLR contiguous region. The threshold value of $r_s > 0.20$ was determined on many tests performed in the application of the algorithm. Implicit in the spatial correlation assumption is that a TICA event ends when $r_s < 0.20$. However, it is important to realize that the algorithm keeps track of the entire history of correlations of any given OLR contiguous region with all other OLR anomaly features in succeeding images. The history of correlations allows one to flag splits in the OLR contiguous regions and also to check the evolution of the sequence regardless of the minimum r_s value.

The tracking method is repeated for all contiguous regions at the time t_i and starts again for the next pentad map. An important note regarding our choice of minimum size (10 grid points) of OLR features is that this methodology is able to track systems moving with speeds up to 10 m s^{-1} (see section 5 and Fig. 7). Since the average eastward propagation of the MJO is about 4 m s^{-1} (Hendon and Salby 1994; Madden and Julian 1994; Jones and Weare 1996), the approach used here is robust in the sense that it does not miss MJO events.

For each sequence (or evolution) of contiguous OLR anomalies, a number of parameters are reported at each time t_i date, minimum OLR anomaly, OLR variance within the contiguous region, number of clusters with OLR anomaly less than -15 W m^{-2} and total area of the contiguous region. The geographical location of the contiguous OLR region at time t_i is defined in three different ways: geometrical center of the contiguous region (OLR anomaly less than -10 W m^{-2}), geometrical center of the cluster with OLR anomaly less than -15 W m^{-2}, and latitude–longitude of the grid point with minimum OLR anomaly (geometrical center is calculated as the average latitude–longitude of the grid points composing the OLR anomaly feature). In case there is more than one cluster with OLR ≤ -15 W m^{-2}, the cluster with lowest OLR is used. If there is more than one grid point with absolute minimum, the latitude–longitude is determined from the geometrical center of the grid points with OLR equal to the absolute minimum. The thresholds of -10 and -15 W m^{-2} are used to investigate the internal variance of the OLR anomaly features. The propagation speed of the system is defined by the movement of the geometrical center of the OLR contiguous region (OLR anomaly < -10 W m^{-2}). The duration of the sequence is calculated in pentads from the origin to the end of the sequence. The total number of sequences identified in this initial process was equal to 2075 with the understanding that many of these sequences were short lived. In order to limit the number of events that were related to significant intraseasonal variations, three additional conditions were imposed: 1) the duration of the event had to last more than 4 pentads, 2) during the strongest stage of evolution, the minimum OLR anomaly had to be less than -25 W m^{-2}, and 3) the sequence propagated eastward and the final longitude of the sequence was eastward of 50°E. Eastward propagation is defined when the final longitude of the sequence was eastward of the longitude at the beginning of the event. The first two conditions were similarly adopted by WR. A small percentage (eight events) had minor westward propagation as determined by the center of gravity of the system. However, individual visual inspection of these cases showed that these systems were clearly boreal summer ISO events moving from the equatorial Indian Ocean towards India and the slight westward propagation was just a result of the particular trajectory of the geometrical center. These cases are included here for completeness. The sequences satisfying the procedure above are denoted here as TICA occurrences and 110 events were identified in 24 years

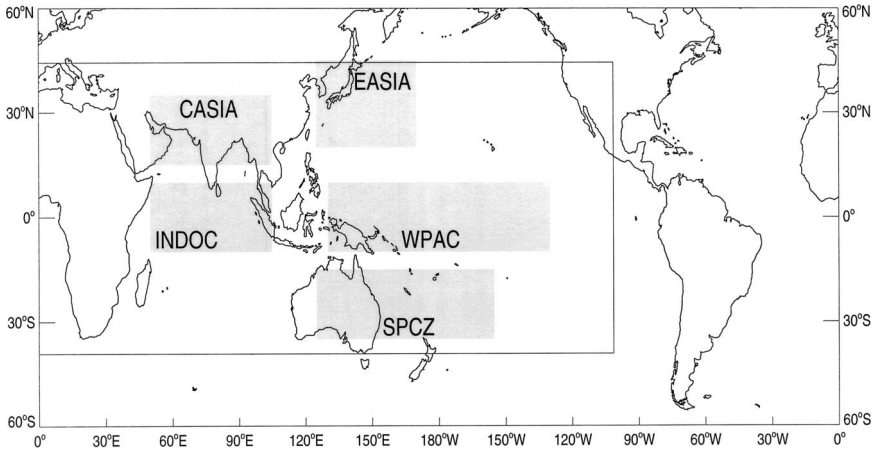

FIG. 1. Domain used to track the trajectories of contiguous regions of OLR anomalies (thin solid lines). The regions indicated by light shading represent the five key areas used to objectively define the propagation of TICA occurrences.

of OLR data. This gives an average of 4–5 events per year, consistent with the MJO (ISO) time scale.

As indicated by WR, actual TICA trajectories reveal more complex behavior than what is derived from other statistical analysis (e.g., EOF, cross-spectral analysis, composites, etc.). In contrast to their methodology, our attempt to characterize TICA trajectories using the latitude/longitude of the grid point with minimum OLR anomaly required frequent subjective decisions. Often, as the OLR contiguous region evolves and changes shape and intensity, the grid point with minimum OLR anomaly moves erratically with large displacements between succeeding pentad maps.

To overcome this difficulty, we developed an alternative procedure to determine TICA trajectories. Five regions in the Indian–Pacific sector are defined (Fig. 1). The selection of these regions was subjective and meant to categorize the 110 events according to distinct trajectories. For any given TICA moving eastward, these regions are used to define the direction of most influential propagation in the following manner. For each time t, MASCOTTE computes the fraction of the contiguous OLR anomaly intersecting each of the five key regions: $R_{L,t}$ for $L = 1, 5$ and $t = 1, T$, where T is the TICA duration. Note that $R_{L,t}$ varies between 0 (if not intersecting region L) and 1 (if fully contained in region L). Next, we define the intersection ratio in region L and time t as

$$F_{L,t} = \frac{R_{L,t}}{\sum_{L=1}^{5} R_{L,t}}. \tag{1}$$

The intersection ratio $F_{L,t}$ is defined as zero, if the denominator in (1) is zero (therefore, $0 \le F_{L,t} \le 1$). For any given TICA sequence, the cumulative intersection ratio (Γ_L) at region L is obtained by integrating $F_{L,t}$ for the duration of the sequence:

$$\Gamma_L = \sum_{t=1}^{T} F_{L,t}. \tag{2}$$

The cumulative intersection ratio (Γ_L) is used as an objective way to determine the most influential direction of propagation as a TICA moves eastward. This parameter essentially takes into account how much of the area of the contiguous OLR anomaly is overlapping with the predefined key regions throughout its life cycle and avoids using a single grid point to determine the propagation direction. Note also that there are no restrictions on the origin of the TICA events. The only conditions are the thresholds of the OLR anomalies and that there is eastward propagation.

Based on the computation of Γ_L, we were able to classify three distinct types of propagation. We determined that significant intersection with a region occurs when $\Gamma_L \ge 1.0$ during the TICA life cycle. Indeed, the ultimate test for validating the entire tracking procedure was to visually inspect the trajectories case by case. The first type denoted as IND includes 19 cases in which the OLR anomaly originates in the Eastern Hemisphere but only intersects the INDOC region in the tropical Indian Ocean (Fig. 1). These cases never fully develop significant eastward propagation towards the western Pacific (WPAC). The second type totals 53 events and is characterized by OLR anomalies that propagate eastward over the Indian Ocean and later move northward toward India and/or eastern Asia (CASIA and EASIA in Fig. 1). As it will be shown next, the majority of these cases occur during boreal spring, summer, and fall, and are called here ISO. The third type typically occurs during boreal winter, when OLR anomalies propagate from the Indian Ocean towards the western Pacific. In this type, OLR anomalies intersect not only the INDOC and WPAC regions but quite often intersect the South Pacific convergence zone (SPCZ) region (Fig. 1). The

algorithm initially identified 40 cases of this type. However, later examination revealed that two of these cases were associated with Kelvin waves, given the excessive propagation speed and were eliminated from this category. Wheeler and Kiladis (1999) provide an extensive discussion of convectively coupled waves in the equatorial region. The remaining 38 cases are called MJO. For convenience, the three types are indicated in Fig. 2.

A quantitative representation is shown in Table 1, which shows the mean cumulative intersection ratio Γ_L for each region and each TICA type. Note that the general features of our classification and the ones obtained by WR are similar but not identical (see their Fig. 5). Some TICA cases originate as one contiguous region of OLR anomaly satisfying the threshold and minimum values criteria specified before. As the contiguous OLR anomaly region moves eastward, a secondary region of OLR anomaly may develop. This secondary OLR region may eventually become separated from the main one (i.e., the values in between the two regions are above the threshold of -10 W m^{-2}) and follow a different trajectory. Our attempts to automatically track the trajectory of the secondary OLR anomaly region required too many subjective decisions. The classification discussed in WR is interesting, since it also gives information about cases that separate in two different trajectories. However, it does not seem practical to subjectively classify these cases when the data sample is large. Therefore our classification emphasizes the trajectory of the main OLR contiguous region as it moves eastward.

To illustrate the propagation characteristics, the following figures show typical cases. Figure 3 shows an ISO case that occurred in May and June of 1982. On 6–10 May, convective anomalies (shaded) developed near Saudi Arabia, whereas a region of convection is still visible over the SPCZ region. In subsequent pentads, the region of enhanced convection intensified over the Indian Ocean and then propagated northward towards the Bay of Bengal and China. The entire duration of this case was 9 pentads and the values of Γ_L were 4.6 (INDOC), 4.3 (CASIA), 0.0 (SPCZ), 0.0 (WPAC), and 0.1 (EASIA), which gives an intuitive feeling for the meaning of Γ_L. A different type of propagation is observed for the MJO example shown in Fig. 4. In late January 1985, convective activity started to develop over equatorial Africa, intensified over the Indian Ocean (10–14 February) and moved to the western Pacific in mid-February–early March. This case, which is a typical boreal winter MJO event, lasted 11 pentads. The values of Γ_L were 2.3 (INDOC), 0.2 (CASIA), 2.6 (SPCZ), 3.9 (WPAC), and 0.0 (EASIA).

4. Seasonal variations

The seasonality of tropical intraseasonal oscillations, and in particular of the MJO, has been explored in many previous studies (Madden and Julian 1994). Salby et al. (1994), for instance, proposed that the seasonal behavior of the MJO is controlled by the latitudinal position of tropical heat sources such that the greatest amplifications occur in the vernal equinox when maximum sea surface temperature (SST) is near the equator. The annual distribution of all TICA events as well as of each TICA category is shown in Fig. 5. The frequency distribution is computed as the ratio of the number of occurrences in the month divided by the total number of events in the category. The distribution of all TICA events (top left) indicates that they are common throughout the year, although higher frequencies are observed in the boreal winter, spring, and fall. The occurrence of IND types shows that they predominantly happen in the boreal winter and spring. The ISO cases frequently occur during the boreal spring, summer, and fall. The highest occurrence, in fact, is observed in spring, which approximately coincides with the transition phase of the Indian monsoon regime. The importance of ISO activity regulating periods of ''active'' and ''breaks'' has been discussed in many previous studies (e.g., Singh et al. 1992; Krishnamurthy and Shukla 2000; Goswami and Mohan 2001). In contrast, the MJO is most frequent during boreal winter. Since the categories adopted in this study and the ones used by WR are not the same and the data record is different, an exact comparison is not possible, although the overall results are consistent with each other.

To obtain more information on the overall annual variability of TICA occurrences, we consider the frequency of occurrence during each seasonal quarter. There are 96 quarters in the available OLR data [24 years of January–February–March (JFM), April–May–June (AMJ), July–August–September (JAS), and October–November–December (OND)]. For each quarter of the year, we counted the number of TICA occurrences regardless of their classification, and thus the quarter frequency is simply the number of quarters with at least one TICA event divided by 24. The frequency of one or more TICA events is quite high during all seasons except JAS when the frequency is considerably lower (Fig. 6).

5. Variations in TICA properties

As explained before, the tracking of TICA events by MASCOTTE registers several properties related to the evolution of the contiguous OLR anomalies. In this section, we examine the possibility of significant differences between ISO and MJO categories. We consider the following properties:

- Duration in pentads.
- Zonal propagation defined as the longitudinal difference between the start and end of the TICA sequence. The start and end are defined by the geometrical center of the cluster with OLR ≤ -15 W m^{-2}.

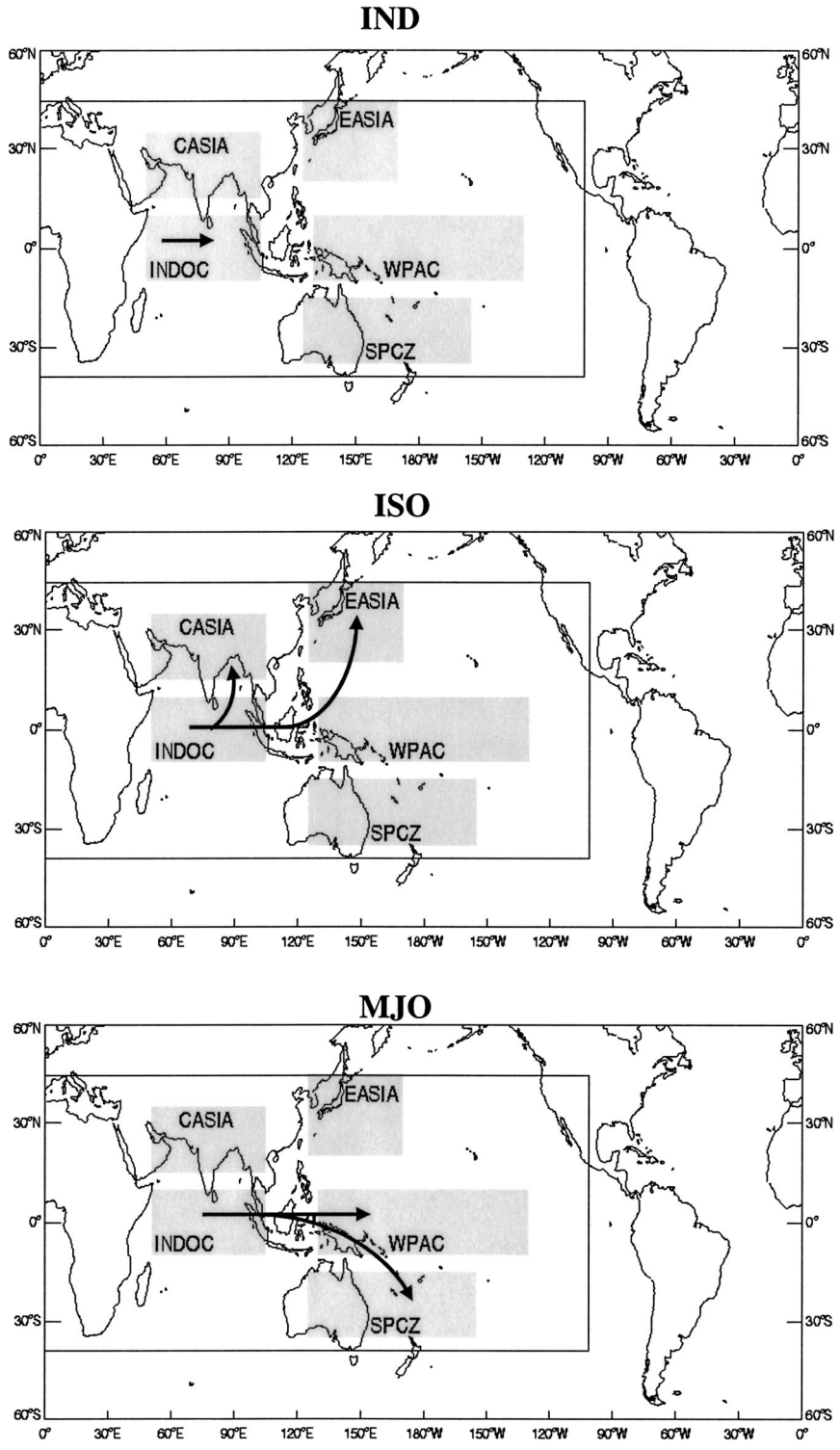

FIG. 2. Schematic representation of the three different types of TICA propagation. The number of events in each category is 19 (IND), 53 (ISO), and 38 (MJO). The total is 110 events.

TABLE 1. Mean cumulative intersection ratio (Γ_L). The total N is 110. See text for explanation.

		Mean cumulative intersection ratio				
TICA	N	INDOC	CASIA	SPCZ	WPAC	EASIA
IND	19	3.6	0.3	0.1	0.1	0.1
ISO	53	2.9	1.2	0.3	1.8	1.7
MJO	38	3.8	1.1	1.8	2.2	0.1

- Minimum OLR anomaly during the TICA life cycle.
- Maximum number of clusters with OLR anomalies ≤ -15 W m^{-2}.
- Variance of OLR within the contiguous region during the strongest stage of evolution.
- Propagation speed.
- Growth of OLR anomaly defined as $|(\mathrm{OLR_P} - \mathrm{OLR_S})/(t_\mathrm{P} - t_\mathrm{S})|$ where $\mathrm{OLR_P}$ and $\mathrm{OLR_S}$ are the anomalies at the peak and start of the TICA sequence and the denominator is the interval from the start to peak.
- Decay of OLR anomaly, defined as before, but for the difference from the peak to the end of the TICA sequence.

Figure 7 shows box plots of the properties of ISO and MJO. The statistical significances between differences in properties between ISO and MJO are shown in Table 2. The differences in the means are assessed by testing the Z statistic:

$$Z = \frac{\overline{X_1} - \overline{X_2}}{\sigma_{\overline{X_1}-\overline{X_2}}},$$

where

$$\sigma_{\overline{X_1}-\overline{X_2}} = \sqrt{\frac{\sigma_1^2}{N_1} + \frac{\sigma_2^2}{N_2}}. \quad (3)$$

Values greater or less than ± 1.64 are significant at the 95% level and indicated in bold. As expected, the MJO lasts longer since these events have greater longitudinal displacements. Interestingly, differences in OLR structure are also observed. MJO events reach lower OLR anomaly values and have greater variance inside the contiguous region than the ISO cases. MJO cases also move faster than ISO types with a mean value of about 4 m s^{-1}. Finally, MJO cases grow and decay slower than ISO types.

6. Interannual variability and major MJO events

An important characteristic of the MJO (ISO) is its irregularity from year to year (Madden and Julian 1994; Slingo et al. 1999; Hendon et al. 1999). We begin this section by reporting the interannual distribution of TICA properties determined by our tracking algorithm. For completeness, Figs. 8 and 9 display the occurrence of all ISO and MJO events identified by the tracking analysis. Each figure shows the duration of the event, the minimum OLR anomaly reached during the life cycle, and the propagation speed. The events are registered for the month they were first identified. The irregularity is observed not only in the occurrence, but also in the amplitude of the properties.

It has been noted in previous studies (e.g., Higgins et al. 2000) that the MJO seems to be more active during ENSO-neutral boreal winters. We tested whether or not statistically significant differences in the occurrences of TICA events in different phases of ENSO can be detected. In order to estimate the interannual distribution of TICA occurrences, the following analysis was performed. First, each quarter in the 24-yr period was classified according to cold, neutral, and warm ENSO phase. The classification used is based on the National Centers for Environmental Prediction (NCEP) Climate Prediction Center assessment of reanalyzed SST anomalies along the equator from 150°W to the date line. This analysis resulted in 22 quarters considered as cold phases, 36 quarters neutral, and 38 quarters warm.

Next, the counts of TICA per quarter and by ENSO phase were computed and frequency distributions constructed. Figure 10 shows the distribution of IND, ISO, and MJO categories as functions of ENSO phases. A total of 47.4% of MJOs occurred in neutral as opposed to 34.2% in warm and 18.4% in cold ENSO. A higher frequency of ISO events is also observed in warm and neutral ENSO.

The statistical significance of differences in occurrences was tested in the following way. Table 3 (top) shows the distribution of IND, ISO, and MJO types according to cold, warm, and neutral ENSO phases. Therefore, the proportions of TICAs in different ENSO phases are: cold (23/110), neutral (45/110), and warm (42/110). We computed the test statistic Z for differences in occurrences between (neutral, cold), (warm, cold), and (warm, neutral) as

TABLE 2. Significance test for difference between means of MJO and ISO characteristics. Differences statistically significant at 95% level are indicated in bold.

	Differences in MJO and ISO properties							
	Duration	D_lon	$\mathrm{OLR_{min}}$	N_{15}	$\mathrm{OLR_{var}}$	Grow	Decay	Speed
$\overline{X_1} - \overline{X_2}$	2.71	53.34	−3.31	0.28	15.43	−1.54	−2.03	0.66
$\sigma_{\overline{X_1}-\overline{X_2}}$	0.65	8.38	1.58	0.21	6.59	0.87	1.07	0.25
Z	**4.13**	**6.36**	**−2.09**	1.28	**2.34**	**−1.77**	**−1.91**	**2.65**

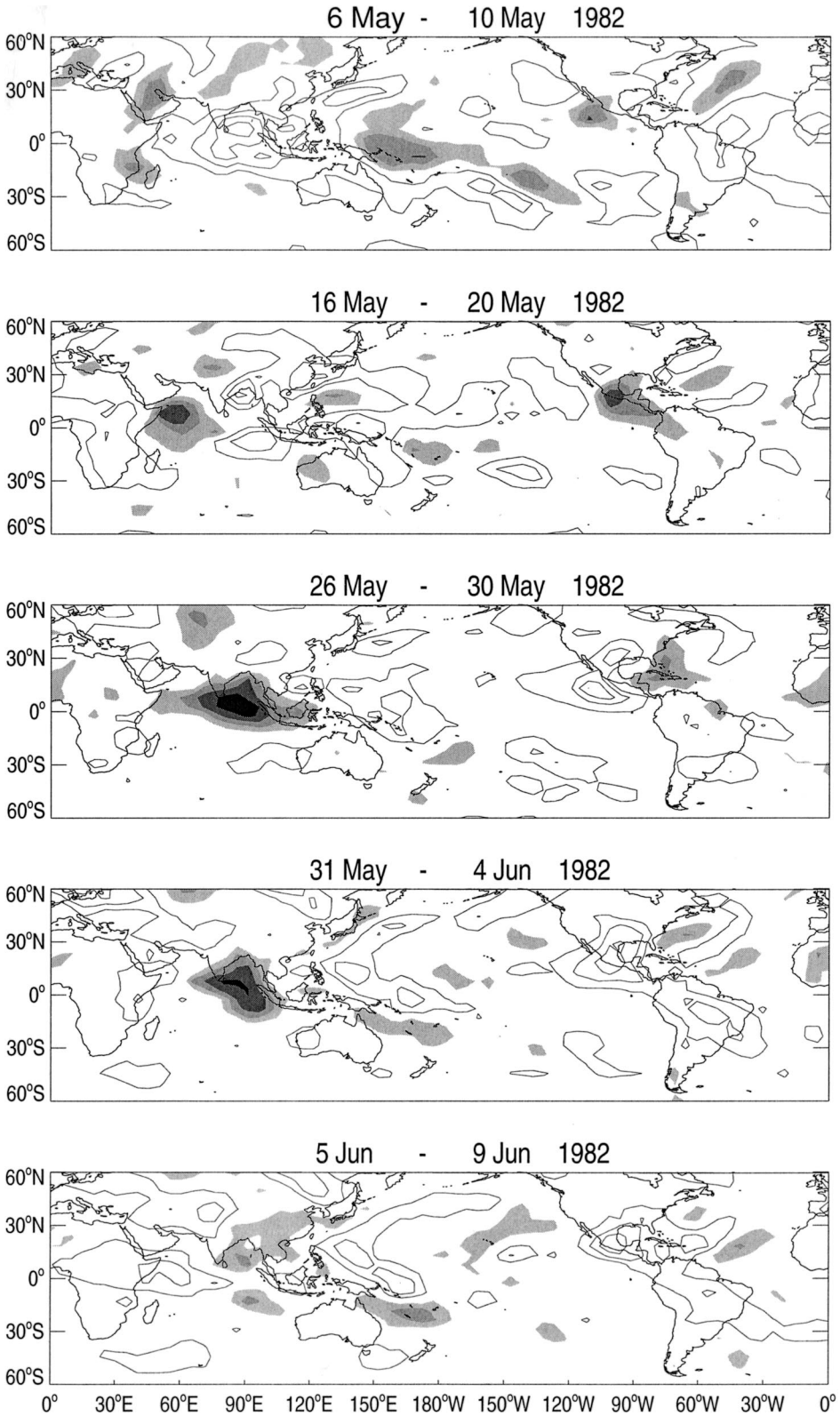

FIG. 3. Example of ISO type of TICA. Dates are indicated in each panel. OLR anomalies less than −10 W m^{-2} are shaded in 10 W m^{-2} increments. Positive anomalies are indicated by solid contours starting at 10 W m^{-2} with 10 W m^{-2} intervals.

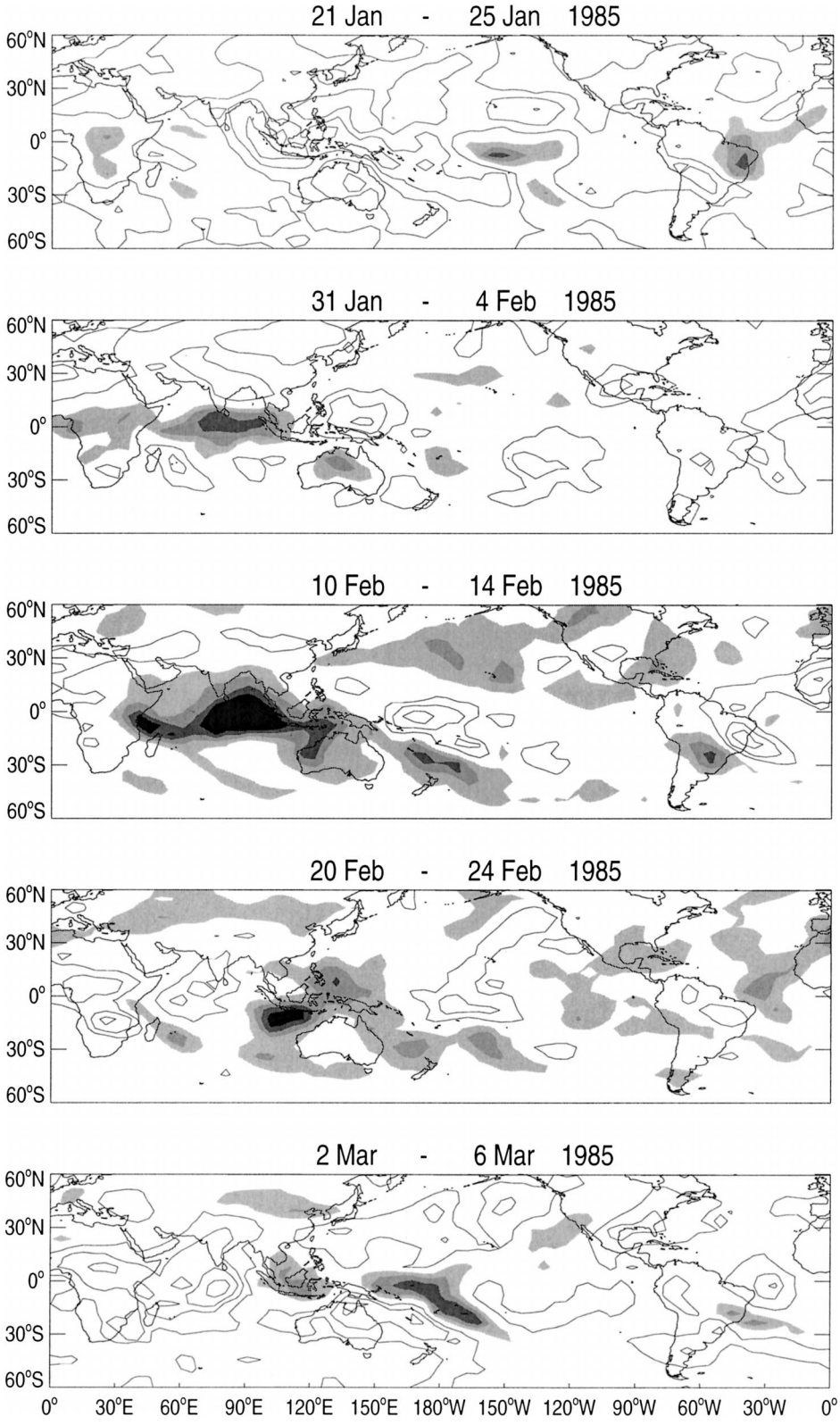

FIG. 4. As in Fig. 3 but for an example of MJO type.

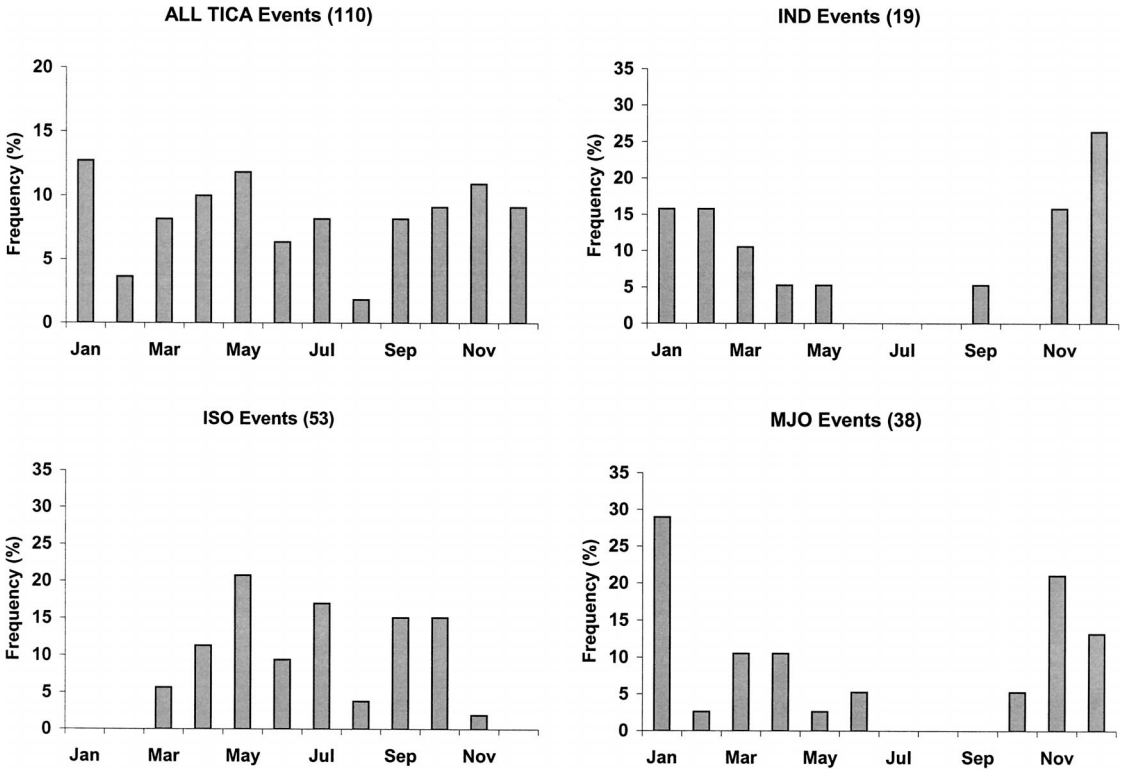

FIG. 5. Seasonal frequency distribution of TICA occurrences: (top left) all TICA types, (top right) IND, (bottom left) ISO, and (bottom right) MJO types. Number of events in each category is indicated in parentheses.

$$Z = \frac{(P_1 - P_2)}{\sqrt{PQ(1/N_1 + 1/N_2)}}. \quad (4)$$

In this expression, P_1 and P_2 are the proportions of occurrence in two ENSO phases, respectively. The standard error of the difference between the two proportions is given by the denominator. Here, $P = (N_1P_1 + N_2P_2)/(N_1 + N_2)$, $Q = 1 - P$, and N_1 and N_2 are the number of quarters in the sample sizes. The null hypothesis is H_0: $P_1 \leq P_2$ and the alternative is H_1: $P_1 > P_2$. The null hypothesis is rejected if the sample proportion P_1 is much greater than the sample proportion P_2 (see Anderson and Finn 1996, 477–481). The values of the Z statistic are shown in Table 3. Values of Z greater than 1.64 would indicate that the differences between the proportions are statistically significant at the 95% level. The results show that, for the 24 years of data analyzed, the occurrences of TICA events in different ENSO phases are not statistically significant. A much longer data record than the one analyzed here is necessary to conclusively assess this issue.

The ENSO phenomenon is related to substantial spatial changes in the tropical Pacific basin. Although observational studies show that air–sea interaction is significant during the MJO life cycle (Jones et al. 1998; Shinoda et al. 1999; Zhang 2001) and may be an important mechanism for its maintenance (Flatau et al. 1997; Waliser et al. 1999), a direct relationship between

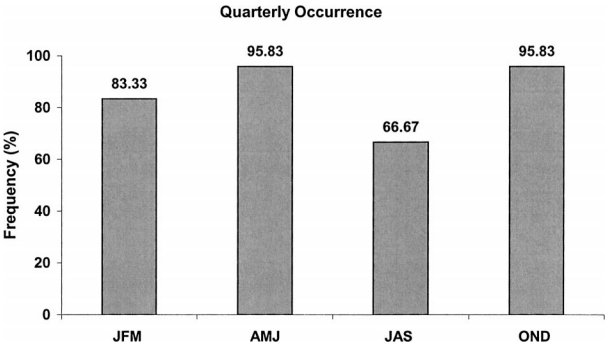

FIG. 6. Quarterly seasonal frequency of TICA events.

TABLE 3. Distribution of TICA events (IND, ISO, and MJO) according to ENSO phases. See text for explanation of statistical test.

	All	IND	ISO	MJO
Cold	23	4	12	7
Warm	42	7	22	13
Neutral	45	8	19	18
Total	110	19	53	38
	P_1 (N_1)	P_2 (N_2)	Z	
Neutral vs cold	45/110 (36)	23/110 (22)	1.568	
Warm vs cold	42/110 (38)	23/110 (22)	1.384	
Warm vs neutral	42/110 (38)	45/110 (36)	−0.240	

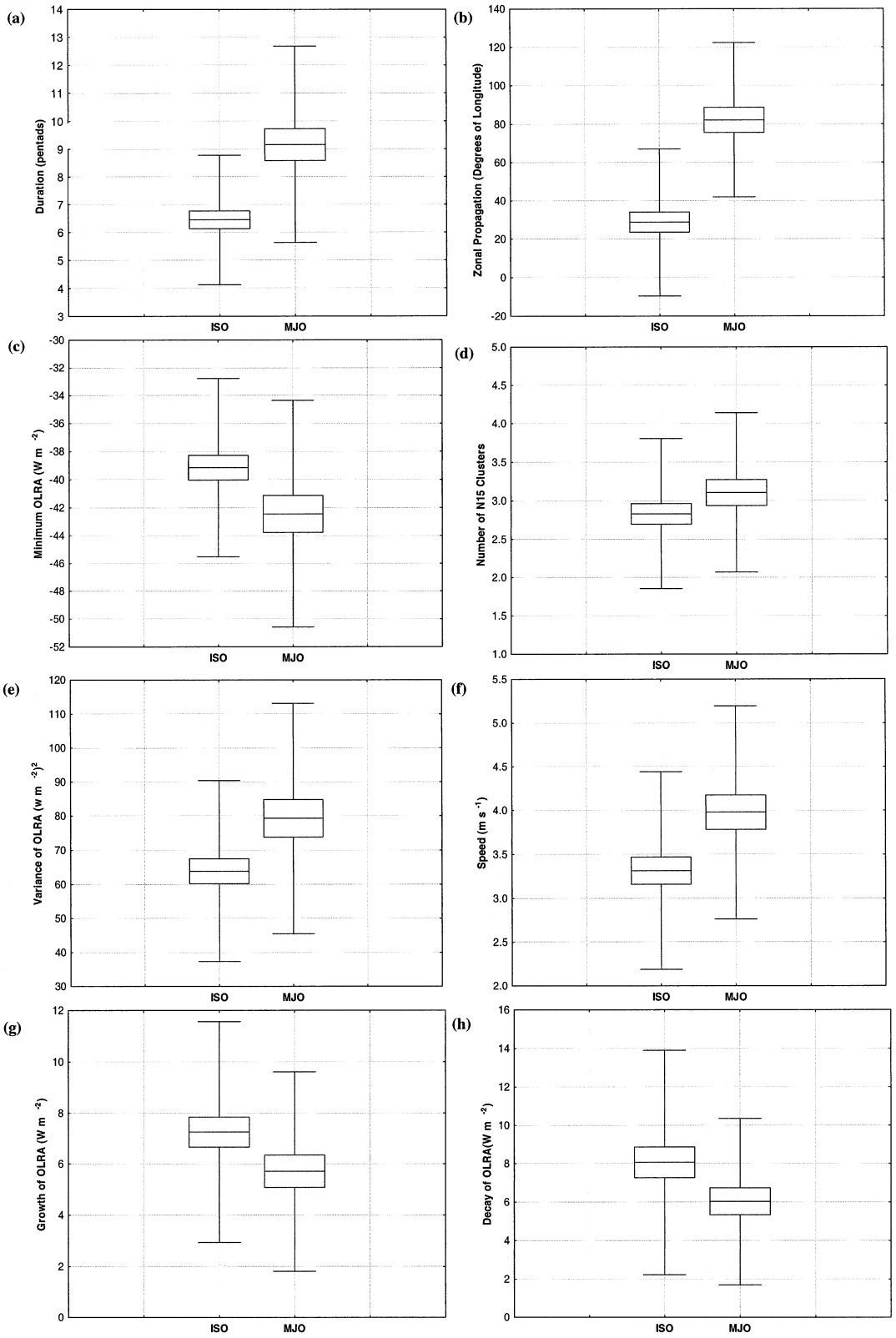

FIG. 7. Box plots representing the distributions of characteristics of ISO and MJO types. The mean value is indicated by a horizontal line surrounded by the standard error (box). The top and lower horizontal lines indicate the range (whiskers) defined in terms of standard deviations. See text for explanations on the determination of the characteristics.

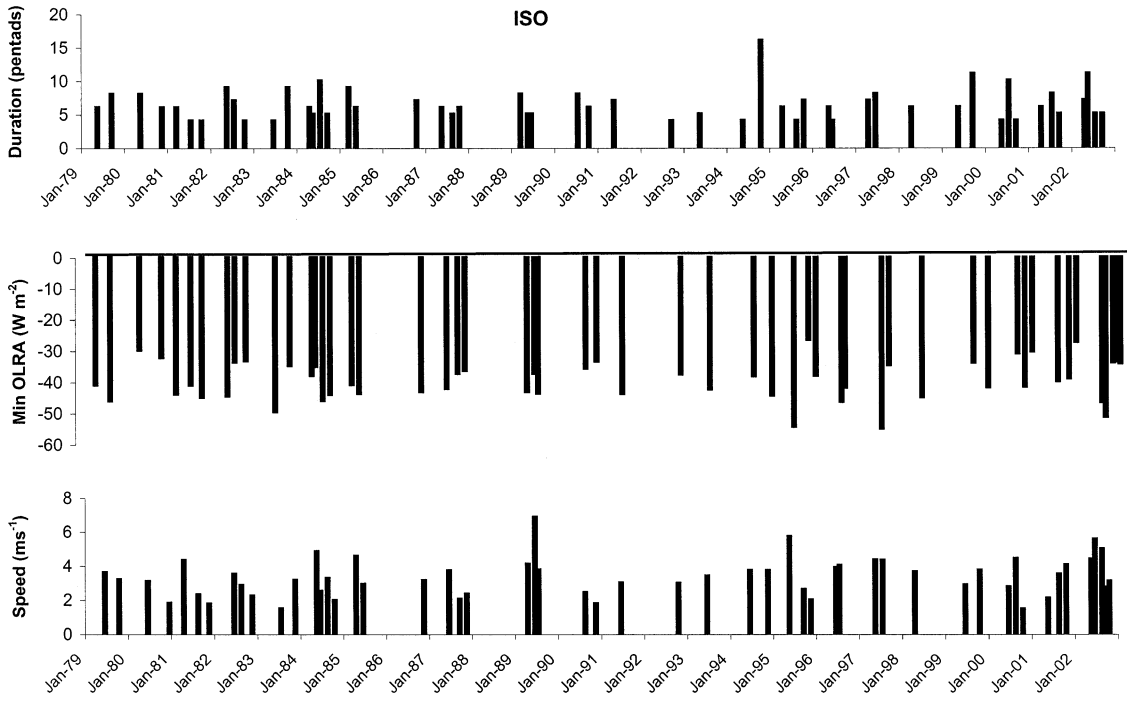

FIG. 8. Temporal distribution of ISO occurrences in terms of (top) duration, (middle) minimum OLR anomaly during the life cycle, and (bottom) propagation speed. Events are recorded in the month they were first identified by MASCOTTE.

interannual variations in tropical Pacific SST and changes in the MJO is less clear (Fink and Speth 1997; Slingo et al. 1999; Hendon et al. 1999; Waliser et al. 2001; Zhang and Gottschalck 2002). Figure 11 displays the temporal occurrence of MJO events and their zonal propagation, that is, the start and end longitudes of the geometrical center of the cluster with OLR ≤ -15 W m^{-2}. The gray color bar indicates the occurrence of cold

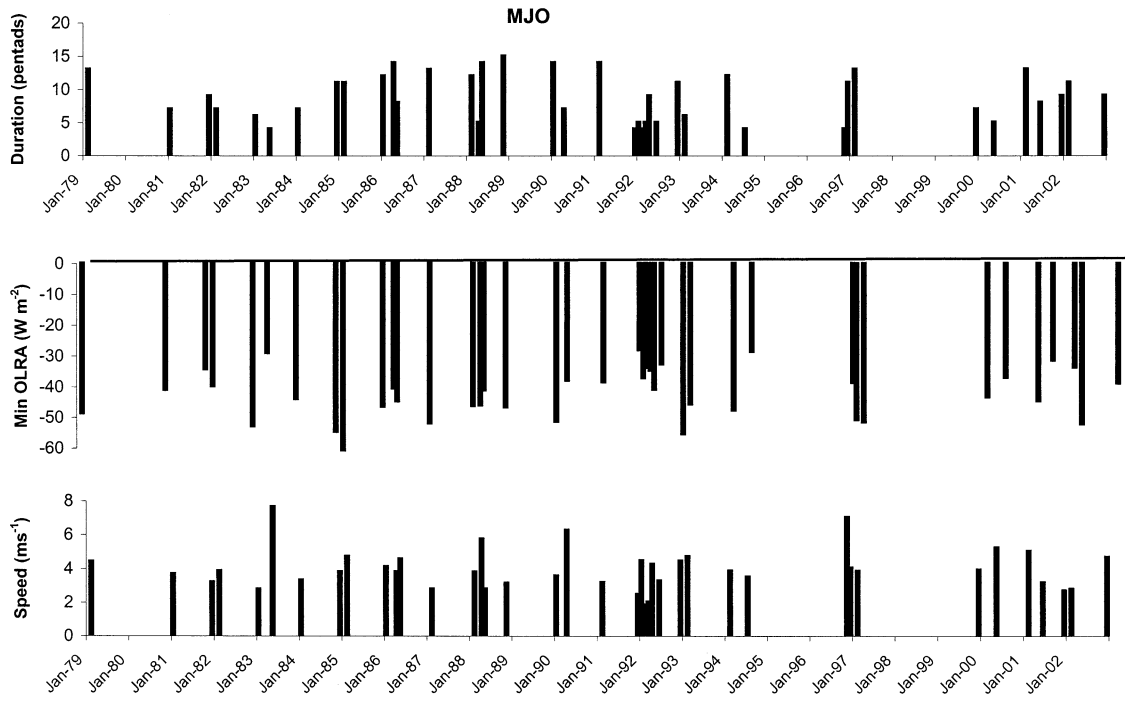

FIG. 9. As in Fig. 8 but for temporal distribution of MJO events.

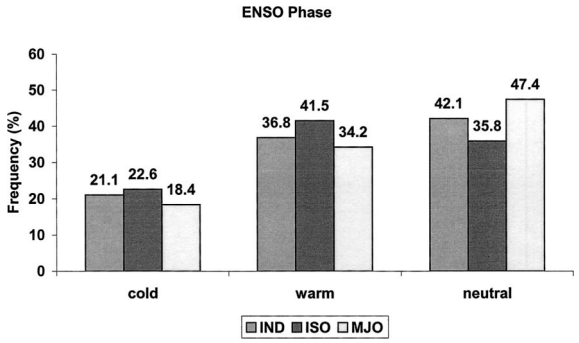

FIG. 10. Distribution of different TICA categories as functions of ENSO phases.

(medium), neutral (light), and warm (dark) ENSO phases. Also indicated is the eastern edge of the western Pacific warm pool (dashed line), determined by the equatorial longitude of the 28°C isotherm. Some studies have indicated that, as the Pacific warm pool expands eastward, tropical intraseasonal disturbances propagate farther east into the equatorial Pacific Ocean (Weickmann 1991; Slingo et al. 1999; Gualdi et al. 1999). While this observation seems to hold for several cases, the magnitude of the zonal propagation does not seem to have an obvious relationship with ENSO.

The importance of the MJO in modulating the structure of the thermocline in the equatorial Pacific Ocean by means of westerly wind bursts and forced oceanic Kelvin waves has been noted in many previous studies (e.g., Kessler et al. 1995; Hendon et al. 1998). In fact, some theoretical results suggest that the MJO may act as a stochastic forcing of ENSO. The study of Kessler and Kleeman (2000), for instance, suggests a rectification mechanism of the MJO into the ENSO cycle. Westerly wind bursts can induce SST anomalies in the Pacific basin that can spawn additional bursts and interact constructively with the ENSO cycle. However, an important characteristic of the MJO is the large degree of variability from event to event and seasonal-to-interannual changes. Although it is not the intent of this study to investigate the interaction of the MJO with the tropical Pacific thermocline structure, this paper examines two relevant questions related to the climatology of the MJO. First, what is the *frequency* of *major* MJO events? In this context, it is clear that not all major MJO events may necessarily have the correct low-level spatial structure to have a significant impact in the tropical Pacific thermocline. Therefore, another important question is: what is the *probability* that a major MJO event has a *potential impact* in the western Pacific?

Before examining the first question, some comments regarding how to define major MJO events are appropriate. A large majority of previous statistical studies of the MJO tend to identify periods of high (low) intraseasonal activity by examining the amplitude of indexes. The indexes can be, for example, filtered time series in predefined locations (Hendon and Salby 1994) or some combination of the first two principal components from empirical orthogonal functions (EOFs) (Jones and Weare 1996; Hendon et al. 1998; Jones 2000; Kessler 2001; Shinoda and Hendon 2002). Although this approach is useful, the amplitude of indexes does not represent events with different properties. For instance, the above technique does not necessarily separate intense events with small zonal propagation from intense events with substantial eastward propagation or different types of trajectories. The advantage of characterizing TICA events according to their propagation characteristics is that these properties can be used to define major events as well.

The frequency distribution of duration, zonal propagation, and minimum OLR anomaly during the life cycle of all 38 MJO events identified in the 24-yr record is displayed in Fig. 12. The median values are 9 pentads, 78.86° of longitude and -43.2 W m^{-2}, respectively. We define here major MJO events as those in which the zonal *displacement* and *lowest* OLR anomaly during the life cycle exceed the corresponding median values. A total of 13 events or 34.21% of MJO's satisfy the criteria. It is interesting to recall that, although the likelihood that a TICA event will occur at any point in the annual cycle is rather high (Fig. 6), the frequency of major MJO events is considerably lower.

The next question is the likelihood that major MJO events may potentially impact the western Pacific warm pool. In order to better separate the major MJO events that may have significant low-level structure, we followed a procedure similar to Shinoda and Hendon (2002), who investigated the rectification effect of the MJO-induced low-level wind speed in the western Pacific. Time series of surface zonal (U) and meridional (V) wind components from NCEP–National Center for Atmospheric Research (NCAR) reanalysis (Kalnay et al. 1996) from 1–5 January 1979 through 27–31 December 2002 were used. First, two low-pass filters were applied to the U and V time series to retain periods longer than 30 and 90 days. Next, the filtered wind speeds were computed as: $\mathrm{WS}_{30} = \sqrt{U_{30}^2 + V_{30}^2}$ and $\mathrm{WS}_{90} = \sqrt{U_{90}^2 + V_{90}^2}$. Shinoda and Hendon (2002) define the increased wind speed produced by intraseasonal variations (or rectification effect due to intraseasonal variations) as: $\mathrm{IWS} = \mathrm{WS}_{30} - \mathrm{WS}_{90}$. They found that during active MJO periods, the wind speed is increased by about 1 m s^{-1} south of the equator in the western Pacific.

Table 4 lists the initial day, month, and year of the 13 major MJO events. Also shown is the ENSO phase during the start of the event, the duration, zonal propagation, and minimum OLR anomaly during the life cycle. The increased wind speed, spatially averaged in the warm pool (15°S–5°N; 130°E–180°), when enhanced convective anomaly was over the region is also included in the table. Six of the major events occurred in neutral,

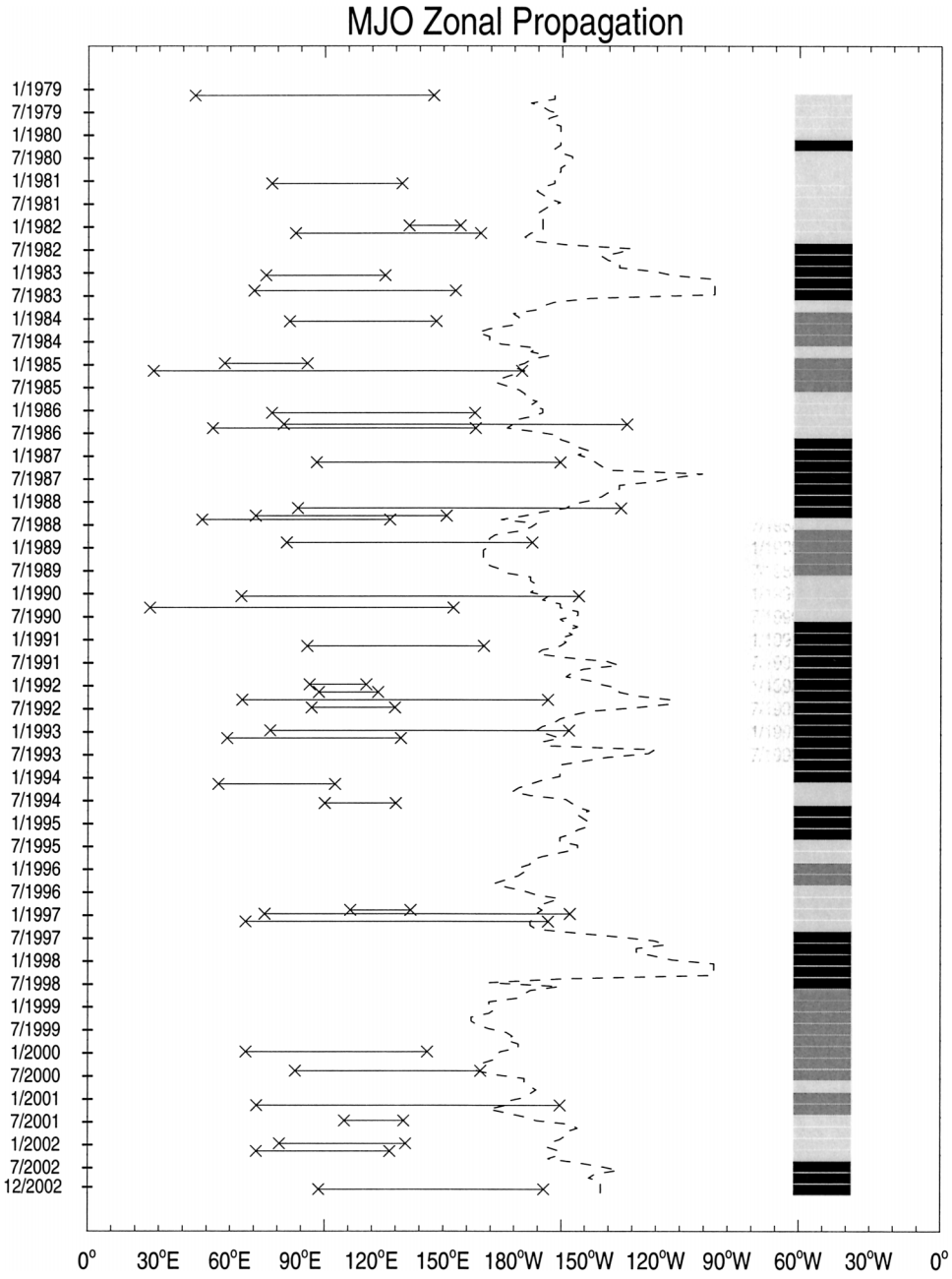

FIG. 11. Temporal distribution of zonal propagation of MJO events (horizontal lines). The gray color bar indicates the occurrence of cold (medium), neutral (light), and warm (dark) ENSO phases. The equatorial eastern edge of the western Pacific warm pool (28°C isotherm) is shown by the dashed line.

four in warm, and three in cold ENSO. The median value of the increased wind speed during the 13 events is equal to 1.95 m s^{-1}. If one considers that a major MJO event may have an impact in the western Pacific warm pool when the increased wind speed is above the median value, then nine events (or 69.23%) are identified (indicated in bold). Although the above normal increased wind speed does not necessarily imply a substantial effect in the thermocline structure in the tropical Pacific, the statistics shown in Table 3 further indicate additional variability among major MJO events. In addition, the vertical temperature structure of the mixed layer and thermocline region can be very important in determining the magnitude and even sign of any SST response to enhanced surface wind speeds associated with the MJO.

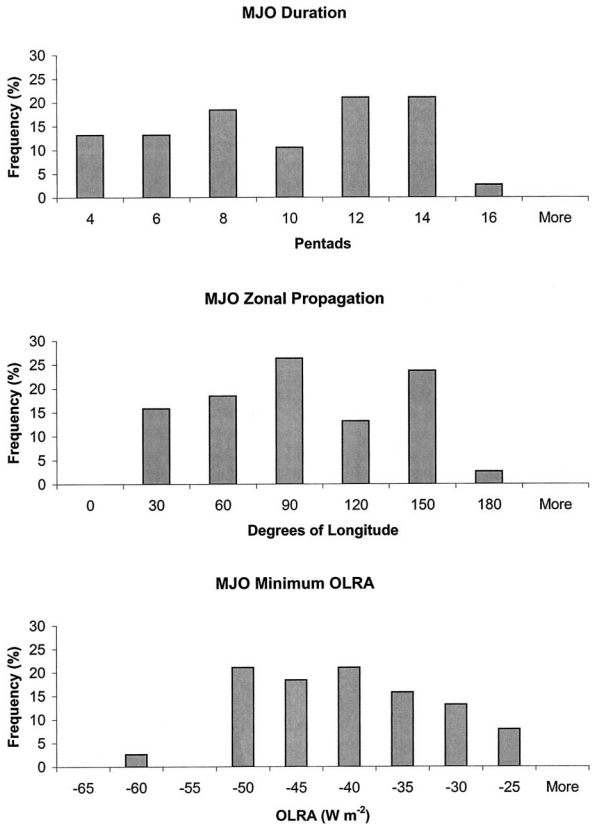

FIG. 12. Frequency distribution of (top) duration, (middle) zonal propagation, and (bottom) minimum OLR anomaly during MJO life cycles.

7. Summary and conclusions

Tropical intraseasonal variations have a central role in subseasonal changes in the coupled ocean–atmosphere system including teleconnections with midlatitudes of both hemispheres. This paper developed an improved climatology by focusing on events that propagate eastward (defined here as TICA). The identification and characterization of TICA events was performed using 24 years of OLR data and the MASCOTTE tracking algorithm. The methodology developed in this study identifies the propagation of TICA events utilizing a procedure that is based on the intersection of the contiguous OLR anomaly with five predefined key regions in the Indian–Pacific sector. The additional advantage of the procedure adopted in this work is the characterization of properties of OLR anomaly features and their evolution. Three distinct types of TICA occurrences were identified. The first type (IND) develops in the Indian Ocean without significant propagation to the western Pacific. For convenience, the second and third types are denominated as ISO and MJO. Some of the findings of this work are similar to the previous study of WR, who used a different procedure to characterize TICA events. TICA events closely related to MJO features are frequent during boreal winter, whereas ISO events are typical during boreal summer. In addition, MJO events last longer, have greater longitudinal displacements, reach lower OLR anomaly values and have greater variance inside the contiguous region than the ISO cases.

The most important contribution of this study is the determination of interannual occurrences of TICA events, an issue that was not examined in the previous study of WR because of the small data record. Although the frequency of MJO (ISO) events seems to be higher during ENSO neutral or ENSO warm events, the data record analyzed in this study does not indicate statistically significant differences. This is closely related to the different frequency of cold, neutral, and warm events in the 24 years of data. A much longer data record is necessary to reliably address this issue.

Although the frequency of TICA events is rather high throughout the year, the occurrence of major MJO events is significantly lower. Major MJO events were defined as those that exceed the median values of zonal propagation and minimum OLR anomaly intensity. A total of 13 events or 34.21% of MJO's identified in the 24

TABLE 4. Major MJO events. Day, month, and year refer to the date when the event was first identified by MASCOTTE. Events marked in bold are major events in which the increased wind speed is above the median value of 1.95 m s^{-1}.

Day	Month	Year	ENSO	Duration (pentads)	Zonal propagation (degrees lon)	Minimum OLR anomaly (W m^{-2})	Increased wind speed (m s^{-1})
16	1	1979	Neutral	13	100.83	−48.31	1.81
21	**1**	**1985**	**Cold**	**11**	**155.56**	**−60.23**	**2.79**
22	**12**	**1985**	**Neutral**	**12**	**85.67**	**−45.97**	**2.14**
6	4	1986	Neutral	8	111	−44.23	1.24
1	1	1987	Warm	13	102.86	−51.43	1.89
11	**1**	**1988**	**Warm**	**12**	**136.5**	**−45.76**	**3.22**
12	3	1988	Warm	5	80.59	−45.57	1.95
28	**10**	**1988**	**Cold**	**15**	**103.75**	**−46.15**	**2.59**
12	**12**	**1989**	**Neutral**	**14**	**142.68**	**−50.88**	**2.94**
27	**11**	**1992**	**Warm**	**11**	**126.24**	**−54.9**	**2.94**
22	**11**	**1996**	**Neutral**	**11**	**129**	**−50.26**	**2.74**
16	**1**	**1997**	**Neutral**	**13**	**127.79**	**−51.01**	**4.56**
1	**1**	**2001**	**Cold**	**13**	**128.23**	**−44.18**	**2.07**

years of data satisfy the criteria. Since not all major MJO events may have the same low-level wind structure and therefore have the same impact in the thermocline of the tropical Pacific, this study also estimated the increased wind speed due to intraseasonal variations (or rectification wind effect). A total of 69.23% of the major MJO events displayed increased wind speeds above the median value.

A major difficulty for operational meteorology is the inability of most dynamical models to realistically represent the MJO (Slingo et al. 1996). In this study, we identified events, denoted IND, that propagate in the Indian Ocean without fully developing significant eastward propagation into the western Pacific Ocean. A comparison of the environmental conditions (i.e., thermodynamic and dynamic) between the IND and MJO types may provide important clues about the necessary conditions for eastward propagation in the Indian–Pacific sector.

In recent years, there has been an increasing interest in the exploration of subseasonal predictability. In this regard, tropical intraseasonal variations play a key role and there is a major effort to determine the empirical and dynamical limit of predictability of the MJO (Waliser et al. 2003). Another motivation for conducting this climatological study of TICA occurrences is to assess the empirical forecast skill of TICA events with different propagation characteristics (i.e., MJO and ISO) as well as possible dependences on interannual time scales. These issues are investigated in a separate work by Jones et al. (2002).

Acknowledgments. The authors would like to acknowledge the support of the National Center for Atmospheric Research (NCAR) and the Climate Prediction Center for making datasets available. NCAR is sponsored by the National Science Foundation. This study benefited from the following research grants—C. Jones: NOAA Office of Global Programs CLIVAR–Pacific Program (NA16GP1019), CLIVAR-PACS (NA16GP1020), and the National Science Foundation (ATM-0094387); D. E. Waliser: NOAA Office of Global Programs CLIVAR (NA16GP2021) and the National Science Foundation (ATM-0094416). Comments and suggestions from anonymous reviewers are greatly appreciated.

REFERENCES

Anderson, T. W., and J. D. Finn, 1996: *The New Statistical Analysis of Data.* Springer-Verlag, 712 pp.

Carvalho, L. M. V., and C. Jones, 2001: A satellite method to identify structural properties of mesoscale convective systems based on maximum spatial correlation tracking technique (MASCOTTE). *J. Appl. Meteor.,* **40,** 1683–1701.

——, ——, and B. Liebmann, 2004: The South Atlantic Convergence Zone: Intensity, form, persistence, and relationships with intraseasonal to interannual activity and extreme rainfall. *J. Climate,* **17,** 88–108.

Chelliah, M., and P. Arkin, 1992: Large-scale interannual variability of monthly outgoing longwave radiation anomalies over the global Tropics. *J. Climate,* **5,** 371–389.

Ferranti, L., T. N. Palmer, F. Molteni, and K. Klinker, 1990: Tropical–extratropical interaction associated with the 30–60 day oscillation and its impact on medium and extended range prediction. *J. Atmos. Sci.,* **47,** 2177–2199.

Fink, A., and P. Speth, 1997: Some potential forcing mechanisms of the year-to-year variability of the tropical convection and its intraseasonal (25–70 day) variability. *Int. J. Climatol.,* **17,** 1513–1534.

Flatau, M., P. J. Flatau, P. Phoebus, and P. P. Niiler, 1997: The feedback between equatorial convection and local radiative and evaporative processes: The implications for intraseasonal oscillations. *J. Atmos. Sci.,* **54,** 2373–2386.

Goswami, B. N., and R. S. A. Mohan, 2001: Intraseasonal oscillations and interannual variability of the Indian summer monsoon. *J. Climate,* **14,** 1180–1198.

Gualdi, S., A. Navarra, and G. Tinarelli, 1999: The interannual variability of the Madden–Julian Oscillation in an ensemble of GCM simulations. *Climate Dyn.,* **15,** 643–658.

Hendon, H. H., and M. L. Salby, 1994: The life cycle of the Madden–Julian oscillation. *J. Atmos. Sci.,* **51,** 2225–2237.

——, B. Liebmann, and J. D. Glick, 1998: Oceanic Kelvin waves and the Madden–Julian oscillation. *J. Atmos. Sci.,* **55,** 88–101.

——, C. Zhang, and J. D. Glick, 1999: Interannual variation of the Madden–Julian oscillation during austral summer. *J. Climate,* **12,** 2538–2550.

Higgins, R. W., and W. Shi, 2001: Intercomparison of the principal modes of interannual and intraseasonal variability of the North American monsoon system. *J. Climate,* **14,** 403–417.

——, J.-K. E. Schemm, W. Shi, and A. Leetmaa, 2000: Extreme precipitation events in the western United States related to tropical forcing. *J. Climate,* **13,** 793–820.

Jones, C., 2000: Occurrence of extreme precipitation events in California and relationships with the Madden–Julian oscillation. *J. Climate,* **13,** 3576–3587.

——, and B. C. Weare, 1996: The role of low-level moisture convergence and ocean latent heat flux in the Madden and Julian oscillation: An observational analysis using ISCCP data and ECMWF analyses. *J. Climate,* **9,** 3086–3104.

——, and L. M. V. de Carvalho, 2002: Active and break phases in the South American monsoon system. *J. Climate,* **15,** 905–914.

——, D. E. Waliser, and C. Gautier, 1998: The influence of the Madden–Julian oscillation on ocean surface heat fluxes and sea surface temperature. *J. Climate,* **11,** 1057–1072.

Kalnay, E., and Coauthors, 1996: NCEP/NCAR 40-Year Reanalysis Project. *Bull. Amer. Meteor. Soc.,* **77,** 437–471.

Kessler, W. S., 2001: EOF representations of the Madden–Julian oscillation and its connection with ENSO. *J. Climate,* **14,** 3055–3061.

——, and R. Kleeman, 2000: Rectification of the Madden–Julian oscillation into the ENSO cycle. *J. Climate,* **13,** 3560–3575.

——, M. J. McPhaden, and K. M. Weickmann, 1995: Forcing of intraseasonal Kelvin waves in the equatorial Pacific. *J. Geophys. Res.,* **100,** 10 613–10 631.

Krishnamurthy, V., and J. Shukla, 2000: Intraseasonal and interannual variability of rainfall over India. *J. Climate,* **13,** 4366–4377.

Lau, K. M., and P. H. Chan, 1986: Aspects of the 40–50 day oscillation during the northern summer as inferred from outgoing longwave radiation. *Mon. Wea. Rev.,* **114,** 1354–1367.

——, and F. C. Chang, 1992: Tropical intraseasonal oscillation and its prediction by the NMC operational model. *J. Climate,* **5,** 1365–1378.

Lucas, L. E., D. E. Waliser, P. Xie, J. E. Janowiak, and B. Liebmann, 2001: Estimating the satellite equatorial crossing time biases in the daily, global outgoing longwave radiation dataset. *J. Climate,* **14,** 2583–2605.

Madden, R. A., and P. R. Julian, 1994: Observations of the 40–50-day tropical oscillation: A review. *Mon. Wea. Rev.,* **122,** 814–837.

Mo, K. C., 2000: Intraseasonal modulation of summer precipitation over North America. *Mon. Wea. Rev.,* **128,** 1490–1505.
Nogués-Paegle, J., L. A. Byerle, and K. Mo, 2000: Intraseasonal modulation of South American summer precipitation. *Mon. Wea. Rev.,* **128,** 837–850.
Rasmusson, E. M., and P. A. Arkin, 1993: A global view of large-scale precipitation variability. *J. Climate,* **6,** 1495–1522.
Salby, M. L., R. R. Garcia, and H. H. Hendon, 1994: Planetary-scale circulations in the presence of climatological and wave-induced heating. *J. Atmos. Sci.,* **51,** 2344–2367.
Shinoda, T., and H. H. Hendon, 2002: Rectified wind forcing and latent heat flux produced by the Madden–Julian oscillation. *J. Climate,* **15,** 3500–3508.
——, ——, and J. D. Glick, 1999: Intraseasonal surface fluxes in the tropical western Pacific and Indian Oceans from NCEP reanalyses. *Mon. Wea. Rev.,* **127,** 678–693.
Singh, S. V., R. H. Kripalani, and D. R. Sikka, 1992: Interannual variability of the Madden–Julian oscillations in Indian summer monsoon rainfall. *J. Climate,* **5,** 973–978.
Slingo, J. M., and Coauthors, 1996: Intraseasonal oscillations in 15 atmospheric general circulation models: Results from an AMIP diagnostic subproject. *Climate Dyn.,* **12,** 325–357.
——, D. P. Rowell, K. R. Sperber, and F. Nortley, 1999: On the predictability of the interannual behaviour of the Madden–Julian oscillation and its relationship with El Niño. *Quart. J. Roy. Meteor. Soc.,* **125,** 583–609.
Waliser, D. E., N. E. Graham and C. Gautier, 1993: Comparison of the highly reflective cloud and outgoing longwave datasets for use in estimating tropical deep convection. *J. Climate,* **6,** 331–353.
——, K. M. Lau, and J.-H. Kim, 1999: The influence of coupled sea surface temperatures on the Madden–Julian oscillation: A model perturbation experiment. *J. Atmos. Sci.,* **56,** 333–358.
——, Z. Zhang, K. M. Lau, and J. H. Kim, 2001: Interannual sea surface temperature variability and the predictability of tropical intraseasonal variability. *J. Atmos. Sci.,* **58,** 2595–2614.
——, K. M. Lau, W. Stern, and C. Jones, 2003: Potential predictability of the Madden–Julian oscillation. *Bull. Amer. Meteor. Soc.,* **84,** 33–50.
Wang, B., and H. Rui, 1990: Synoptic climatology of transient tropical intraseasonal convection anomalies. *Meteor. Atmos. Phys.,* **44,** 43–61.
Weickmann, K. M., 1991: El Niño/Southern Oscillation and the Madden–Julian (30–60 day) oscillations during 1981–1982. *J. Geophys. Res.,* **96,** 3187–3195.
Wheeler, M., and G. Kiladis, 1999: Convectively coupled equatorial waves: Analysis of clouds and temperature in the wavenumber–frequency domain. *J. Atmos. Sci.,* **56,** 374–399.
Yasunari, T., 1979: Cloudiness fluctuations associated with the Northern Hemisphere monsoon. *J. Meteor. Soc. Japan,* **57,** 225–229.
Zhang, C., 2001: Intraseasonal perturbations in sea surface temperatures of the equatorial eastern Pacific and their association with the Madden–Julian oscillation. *J. Climate,* **14,** 1309–1322.
——, and J. Gottschalck, 2002: SST anomalies of ENSO and the Madden–Julian oscillation in the equatorial Pacific. *J. Climate,* **15,** 2429–2445.